Journal of Materials and Environmental Sciences
ISSN : 2028-2508
CODEN : JMESCN

J. Mater. Environ. Sci., 2018, Volume 9, Issue 4, Page 1234-1246

https://doi.org/10.26872/jmes.2017.9.4.135

http://www.jmaterenvironsci.com

Corrosion Inhibition Effect of Novel Pyrazolo [3,4-d] pyrimidine Derivative on Mild Steel in 1 M HCl Medium: Experimental and Theoretical Approach.

M. El Hafi[1], A. Ezzanad[2], M. Boulhaoua[1], L. El Ouasif[1], M. Saadouni[3], Y. El Aoufir[2,4*], Y. Ramli[5], A. Zarrouk[6], H. Oudda[4], E. M. Essassi[1]

1. Laboratoire de Chimie Organique Hétérocyclique URAC 21, Pôle de Compétences Pharmacochimie, Mohammed V University BP 1014, Avenue Ibn Batouta, Rabat, Morocco.

2. Materials, Nanotechnology and Environment Laboratory, Faculty of Sciences, Mohammed V University Rabat, Morocco.

3. Laboratory of Organic, Organometallic and Theoretical Chemistry, Faculty of Science, Ibn Tofaïl University, 14000 Kenitra, Morocco

4.Laboratory separation processes, Faculty of Science, Ibn Tofail University PO Box 242, Kenitra, Morocco.

5. Laboratoire de Chimie Thérapeutique, Faculté de Médecine et de Pharmacie, Mohammed. V University in Rabat BP 6203, Avenue Mohamed Belarbi El Alaoui, Rabat, Morocco.

6. LCAE-URAC18, Faculté des Sciences, Université Mohammed 1 er, Oujda, Morocco.

Received 01Aug 2017,
Revised 04Oct 2017,
Accepted 11 Oct 2017

Keywords

- ✓ Pyrazolo [3,4-d] pyrimidines;
- ✓ Corroioninhibition;
- ✓ Mildsteel;
- ✓ MolecularDynamic;
- ✓ HCl
- ✓ Electrochemicalmethods

Y. El Aoufir : eyasmina1@gmail.com

Abstract

The inhibitory effect of 1-methyl-4-phenyl-1*H*-pyrazolo[3,4-d]pyrimidine (MPPP) on the corrosion of mild steel in 1 M hydrochloric acid was studied using potentiodynamic polarization technique and electrochemical impedance spectroscopy measurements at 303K. The results indicate that the pyrazolopyrimidine compound with an average efficiency of 93% at 10^{-3} M of additive concentration has fairly effective inhibiting properties for mild steel in hydrochloric acid, and acts as mixed type inhibitor. The inhibition efficiencies measured by all measurements show that the inhibition efficiencies increase with increase in inhibitor concentration. This reveals that the inhibitive mechanism of inhibitor was primarily due to adsorption on mild steel surface, and follow Langmuir adsorption isotherm. The temperature effect on the inhibition process in 1 M HCl with the addition of investigated compound was studied at a temperature range of 303–333 K, and the activation parameters (Ea, ΔH and ΔS) were calculated to elaborate the corrosion mechanism. Molecular dynamic simulations and quantum chemical parameters obtained from density functional theory (DFT) calculations were discussed with experimental results.

1. Introduction

Acid solutions, especially that of hydrochloric acid, are widely used in various industrial processes such as oil well acidification, acid pickling, descaling and others which leads to serious electrochemical corrosion as well as hydrogen embrittlement to the metallic structure[1,2]. Mild steel, on the other hand, is an immensely useful structural material, mostly due to its high tensile strength, ductility, malleability and above all, easy availability. Last few decades have witnessed gradual surge in the works related to managing the acid induced corrosion damage of mild steel. Among various modes of operation in this field, application of various organic inhibitors remains one of active fields of research, mostly due to cost-effectiveness as well as easy applicability[3-7]. Organic compounds containing electronegative functional groups and π e− systems are usually good inhibitors of corrosion for many alloys and metals in corrosive environment. These organic systems can be adsorbed on

the surface of the metal through the hetero atoms such as nitrogen, oxygen and sulfur[8-21]. The structure and properties of the inhibitor molecule such as functional groups, steric factor, molecular size, molecular weight, molecular structure, aromaticity, electron density of the donor atoms and π-orbital character of donating electrons affect the adsorption of corrosion inhibitor on metal surface[22]. On the other hand, theoretical calculations have been used recently to explain the mechanism of corrosion inhibition, which proved to be a very powerful tool in this direction[23]. The geometry of inhibitor molecule in its ground state, nature of its molecular orbitals, HOMO and LUMO are directly involved in the corrosion inhibition activity. Likewise, molecular dynamic simulation is the most authentic technique which has enormous advantages of evaluating microcosmic inhibition performance and exploration of their mechanism. Results obtained from these studies have shed more light into the reactivity, active sites and the mechanism of interaction of these inhibitors with steel surface. These findings help us for rational designing of promising corrosion inhibitors[24,25].
The aim of this work is to study the inhibition effect of 1-methyl-4-phenyl-1*H*-pyrazolo[3,4-d]pyrimidine (MPPP) on the corrosion of mild steel at different concentrations and different temperatures in hydrochloric acid (HCl). Electrochemical investigations were employed for the exploration of inhibition efficiency of this organic compound. Afterward, quantum chemical calculations and MD simulations have been performed to elucidate the effect of their structural and electronic properties in inhibition efficacy.

2. Experimental details

2.1. Synthesis of 1-methyl-4-phenyl-1H-pyrazolo [3,4-d]pyrimidine

To a microwave vial was added 1-methyl-4-chloro-1*H*-pyrazolo[3,4-d]pyrimidine**1** (50 mg, 0.3 mmol), phenylboronic acid (40.23 mg, 0.33 mmol), K_2CO_3 (124.38 mg, 0, 9 mmol) $PdCl_2$(dppf) (22 mg, 0.03 mmol), THF (3ml), and H_2O (10 µL). The reaction mixture was heated with stirring in microwave reactor at 170°C for 10 min. The crude reaction mixture was passed through a small silica gel plug eluting with EtOAc, and the crude material was purified by silica gel chromatography (0 to 10% EtOAc gradient in hexanes) to obtain (49 mg , 0.23 mmol), 80% of 1-methyl-4-phenyl-1*H*-pyrazolo [3,4-d]pyrimidine**2** as white powder ; mp 115-117°C (Scheme 1).

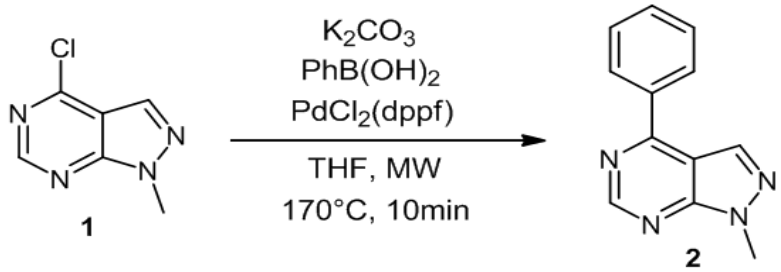

Scheme 1: Synthesis of 1-methyl-4-phenyl-1*H*-pyrazolo [3,4-d]pyrimidine

The compound**2** was characterized by NMR and HRMS. ^{1}H NMR (400 MHz, $CDCl_3$-d) δ : 9.08 (s, 1H), 8.36 (s, 1H), 8.20 (dd, *J* = 6.7, 3.0 Hz, 2H), 7.62 – 7.56 (m, 3H), 4.18 (s, 3H). ^{13}C NMR (101 MHz, $CDCl_3$-d) δ : 160.9, 155.3 , 153.8 , 137.1 , 132.9 , 131.6 , 129.0 (2C) , 129.1 (2C) , 111.6 , 34.2. HRMS (ESI): calcd. for $C_{12}H_{11}N_4$ $[M + H]^+$ 211.0978 ; found 211.0979.

2. 2. Materials and test solution

The steel used in this study is a carbon steel had the following composition (atom %):0.370 % C, 0.230 % Si, 0.680 % Mn, 0.016 % S, 0.077 % Cr, 0.011 % Ti, 0.059 % Ni, 0.009 % Co, 0.160 % Cu and the remainder iron (Fe). For electrochemical studies, 1 cm^2 area was exposed during each measurement. Before measurements the samples were polished using different grades of emery papers SiC (120, 600 and 1200); and then subjected to the action of a buffing machine attached with a cotton wheel and a fiber wheel having buffing soap to ensure mirror bright finish, degreased by washing with ethanol, acetone and finally washed with distilled water.
The aggressive solutions of 1.0 M HCl were prepared by dilution of analytical grade 37% HCl with distilled water. The concentration range of the compound MPPPused was 5×10^{-5} to 1×10^{-3} M.

2.3. Electrochemical tests

Electrochemical tests were carried out in a conventional three electrode cell with platinum counter electrode, saturated calomel electrode as the reference electrode and the carbon steel with the surface area of 1 cm^2 as the

working electrode. Electrochemical experiments were conducted using impedance equipment (Tacussel Radiometer PGZ 100) and controlled with Tacussel corrosion analysis software model Voltamaster 4.
Before electrochemical tests, the working electrode was immersed in test solution at open circuit potential (OCP) for 30 min to attain a stable state. The potential of potentiodynamic polarization curves started from potential -800 mV to -200 mV vs. SCE with a scan rate of 1 mV s^{-1}. Electrochemical impedance spectroscopic studies were carried out at OCP in the frequency range of 10 mHz -100 kHz, with 10 points per decade, at the rest potential, after 30 min of acid immersion, by applying 10 mV peak to peak voltage excitation. Nyquist plots were made from these experiments.

2.4. Theoretical calculations

E_{HOMO} (highest occupied molecular orbital energy), E_{LUMO} (lowest unoccupied molecular orbital energy) and Fukui indices calculations were performed using *DMol*^{3} module in Materials Studio version 6.0[26]. These calculations employed an *ab initio*, gradient-corrected functional (*GGA*) method with a double numeric plus polarization (DNP) basis set and a Becke One Parameter (BOP) functional. It is well-known that the phenomena of electrochemical corrosion appear in aqueous phase. *DMol*^{3} includes certain COSMO controls, which allow for the treatment of solvation effects[27,28].
According to Koopman's theorem [29] the ionization potential (I) and electron affinity (A) of the inhibitors are calculated using the following equations.

$$I = -E_{HOMO} \quad (1)$$

$$A = -E_{LUMO} \quad (2)$$

Thus, the values of the electronegativity (χ) and the chemical hardness (η) according to Pearson, operational and approximate definitions can be evaluated using the following relations[30]:

$$\chi = \frac{I+A}{2} \quad (3)$$

$$\eta = \frac{I-A}{2} \quad (4)$$

The number of transferred electrons (ΔN) was also calculated depending on the quantum chemical method[31-33] by using the equation:

$$\Delta N = \frac{\phi - \chi_{inh}}{2(\eta_{Fe}+\eta_{inh})} \quad (5)$$

The obtained DFT derived ϕ values for Fe (1 0 0), Fe (1 1 0) and Fe (1 1 1) surfaces are 3.91, 4.82 and 3.88 eV, respectively[34,35].In this study, we use only Fe (1 1 0) surface due to its higher stabilization energy and packed surface.
The local reactivity of inhibitor molecules were obtained by condensed Fukui functions[36]. Finite difference approximations have been used to get Fukui functions in favor of nucleophilic and electrophilic attacks as[37]:

$$f_k^+ = q_k(N+1) - q_k(N) \quad (6)$$

$$f_k^- = q_k(N) - q_k(N-1) \quad (7)$$

Here, gross charge of the atom k is denoted by q_k. The $q_k(N+1)$, q_k (N) and q_k $(N-1)$ are the charges of the anionic, neutral and cationic species, respectively.

2.5. MD simulations

MD simulations were performed using discover module Material Studio software 6.0 (from Accelrys Inc.), to model the adsorption behavior of the inhibitor molecule onto Fe (110) surface. The MD simulations were conducted in the three dimensional simulation box (28.55 × 28.55 × 59.16 Å) with periodic boundary condition in order to avoid any arbitrary boundary effects. In this investigation, the constructed simulation box was comprised of three layers. The first layer contain Fe slab, and the second layer was the solution slab which contains water molecule as well as molecular ions like H_3O^+, Cl^- and the remaining part of the box is the vacuum layer. After construction of the simulation box, dynamic simulation was carried out using COMPASS (Condensed Phase Optimized Molecular Potentials for Atomistic Simulation Studies) force filed. All the bulk atoms in Fe (110) surface were kept frozen and all the concerned molecules were allowed to interact with the metallic surface freely during the entire simulation process. The MD simulations were performed at 303 K using canonical ensemble (NVT) with a time step of 1.0 fs and a simulation time of 500 ps. The interaction energy ($E_{interaction}$) between the inhibitor molecule and the Fe (110) surface have been calculated by using the following equation[5]:

$$E_{\text{interaction}} = E_{\text{Total}} - (E_{\text{solution}} + E_{\text{inhibitor}}) \quad (8)$$

where the total energy of the simulation system was defined as E_{total}, the energy of the iron surface together with solution (H_2O, H_3O^+, Cl^-) was classified as $E_{solution}$and the energy of the adsorbed inhibitor molecule as $E_{inhibitor}$.

The binding energy of the inhibitor molecule was the negative value of the interaction energy as follows[3]:

$$E_{\text{Binding}} = E_{\text{interaction}} \quad (9)$$

3. Results and discussion

3.1. Potentiodynamic polarization curves

Polarization measurements have been carried out to pool information concerning the kinetics of anodic and cathodic reactions. The potentiodynamic polarization curves for mild steel in 1 M hydrochloric acid solution in the absence and presence of various concentrations of the inhibitor molecule are shown in Fig. 1. The values of electrochemical kinetic parameters, like corrosion current density (i_{corr}) and Tafel slopes (βa and βc), determined from these graphs by extrapolation method are listed in Table 1. The values of efficiency $\eta_{PDP}(\%)$ are calculated using Eq. 10.

$$\eta_{PDP}(\%) = \frac{i_{corr} - i'_{corr}}{i_{corr}} \times 100 \quad (10)$$

Where i_{corr} and i'_{corr} are the corrosion current densities in uninhibited and inhibited medium, respectively.

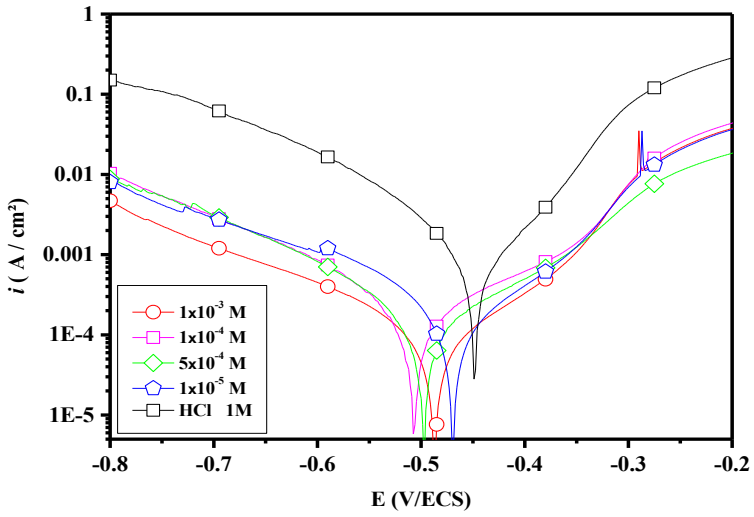

Figure 1: Polarization curves of carbon steel in 1.0 M HCl for various concentrations of MPPP at 303K.

Table 1: Polarization data of carbon steel in 1M HCl without and with various concentrations of MPPP at 303K

Inhibitor	Concentration (M)	-E_{corr} (mV/SCE)	βa (mV dec^{-1})	-βc (mV dec^{-1})	i_{corr} (µA cm^{-2})	η_{PDP} (%)
Blank	1	450	124	96	513	
	10^{-3}	486	78	119	35	93
MPPP	5×10^{-4}	468	88	130	50	90
	10^{-4}	497	157	142	61	88
	10^{-5}	506	194	156	78	84

The inspection of Fig. 1 and Table 1, it is clear that the addition of inhibitor to the acid media affected both the anodic and cathodic parts of the Tafel slopes. Addition of MPPP to acidic medium results in marked decrease in the corrosion current density (i_{corr}). In other words, both anodic metal dissolution and cathodic recations to produce hydrogen gas are drastically inhibited. Furthermore, both anodic (βa) as well as cathodic Tafel (βc) slopes for MPPP were observed to be change with increasing inhibitor concentration, resulting that the investigated inhibitor affects both reactions[38]. Also from Table 1, corrosion current densities decreases with the increase in inhibitor concentration, while the inhibition efficiencies increases as expected.

Data in Table 1, reveals that the addition of inhibitor, slightly shifts the E_{corr} values in negative direction following OCP trend, which strongly suggests that the tested compound may be classified as mixed type inhibitor in HCl solution, suggesting that the addition of inhibitor to a 1 M HCl solution reduces both anodic metal dissolution of mild steel and cathodic hydrogen evolution reaction[39].

3.2 Electrochemical Impedance Spectroscopy Measurements EIS

To confirm the obtained results by potentiodynamic polarization curves and study the inhibition mechanism in more detail, EIS was used. Nyquist plots for mild steel in 1 M HCl after 0.5 hour of immersion time at the corrosion potential in the absence and the presence of MPPP at different concentrations are shown in Fig. 2. In the EIS experiments, with presence and absence of MPPP, only single semicircles are observed with depression at low frequency. This depression is often associated to the non-homogeneity and roughness of the carbon steel surface[40]. A remarkable increase of the depressed semicircle diameter is observed with the presence of MPPP. Generally, the EIS plots, loop-like capacitive is mainly attributed to the charge transfer process, while the increase of semicircle diameter with a rise in MPPP concentration is the result of the adsorption of the inhibitor on the carbon steel surface[41].

Compared to the uninhibited system, nature of the impedance diagrams are seen to remain the same in presence of the inhibitor, suggesting almost no change in the corrosion mechanism due to inhibitor addition[42]. For both the inhibited and uninhibited systems, Bode impedance plots (Fig. 3) exhibit one negative fluctuation, while the Bode phase plots are characterized by only one maximum point (Fig. 3). All these are the characteristics of one time constant only, where the corrosion inhibitive effect by the studied inhibitor is mostly polarization resistance controlled.

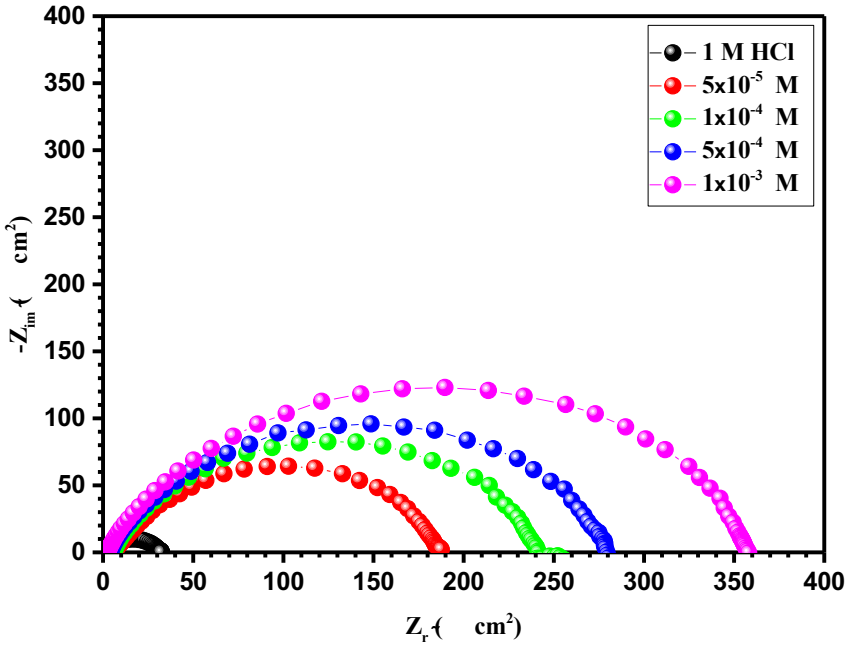

Figure 2: Nyquist diagrams for carbon steel in 1M HCl containing different concentrations of MPPP at 303K.

The equivalent circuit model is shown in Fig. 4 was used to analyse the *EIS* experiments, the parameters are collected in Table 2, while the double layer capacitance (C_{dl}) values are calculated using the Eq. (11):

$$C_{dl} = \sqrt[n]{\mathrm{Q}.\mathrm{R_{ct}}^{1-\mathrm{n}}} \qquad (11)$$

where Q is the *CPE* constant and n is a coefficient that can be used as a measure of surface inhomogeneity[43]. The Eq. (12) was used to calculate the η_{EIS} (%):

$$\eta_{EIS}(\%) = \frac{R_p - R'_p}{R_p} x100 \qquad (12)$$

Where R_p and R'_p are the polarization resistance values in with and without MPPP, respectively.

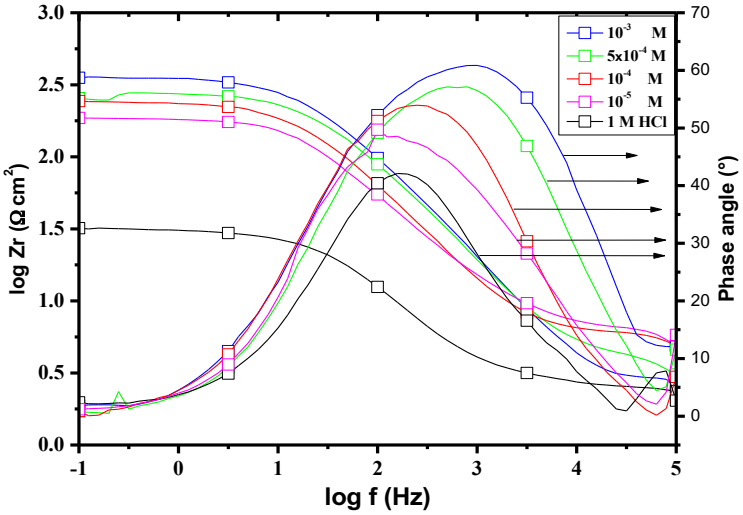

Figure3: Bode (log *f vs.* log |Z|) and phase angle (log *fvs.* Φ) plots of impendence spectra for Carbon steel in 1 M HCl containing 10^{-3} M of MPPP.

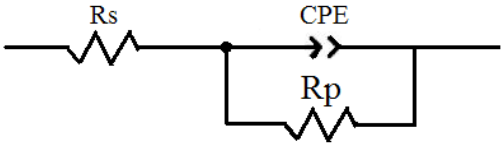

Figure 4: The electrochemical equivalent circuit used to fit the impedance spectra.

Table 2: Impedance parameters for corrosion of carbon steel in 1.0 M HCl in the absence and presence of different concentrations of MPPP at 303 K.

Inhibitor	Concentration (M)	R_{ct} (Ω cm^2)	n	Q×10^{-6} (s^n Ω^{-1}cm^{-2})	C_{dl} (μF cm^{-2})	η_{EIS} (%)
Blank	1	29.04	0.763	557	155	-
MPPP	10^{-3}	354.9	0.777	59.31	19.66	92
	5×10^{-4}	276.4	0.775	65.17	20.31	89
	10^{-4}	236.3	0.783	94.06	32.75	87
	10^{-5}	187.5	0.765	125	40.35	84

Evaluation of Table 2 shows that the values of R_p and C_{dl} have opposite trend at the whole concentration range and it may be due to the formation of a protective layer on the surface of the electrode. The double layer between the charged metal surface and the solution is considered as an electrical double capacitor. The adsorption of inhibitor molecule on carbon steel surface decreases its electrical capacity through the displacement of water molecule and other ions originally adsorbed on the metal surface. The drop off in C_{dl} value may be attributed to a decrease in local dielectric constant or an increase in thickness of the electrical double layer. This may be ascribed to the formation of a protective layer on the carbon steel surface[44] and trim down the extent of dissolution of metal[45]. Adsorption of this molecule occurs because of the interaction energy between the metal surface and the inhibitor is superior to the interaction energy between the metal surface and the water molecules[46].This trend is in accordance with Helmholtz model given by the equation equation(13):

$$C_{dl} = \frac{\sum \sum_0 A}{d} \qquad (13)$$

where d is the thickness of the protective layer, Σ is the dielectric constant of the medium, Σ_0 is the vacuum permittivity and A is the surface area of the electrode.

3.3 Effect of temperature and activation parameters

Temperature has a great effect on the rate of metal electrochemical corrosion. In case of corrosion in an acid medium, the corrosion rate increases exponentially with temperature increase because the hydrogen evolution over potential decreases[47]. Typical polarisation potentiodynamic plots for MS in 1.0 M HCl medium and in the presence of MPPP at temperature ranging from 303 to 333 K are graphically presented in Fig. 5a-b. Table 3 collected the parameters derived from PDP plots. The results reported in Table 3 showed that the i_{corr}values decrease with the increasing temperature in the absence and the presence of MPPP.

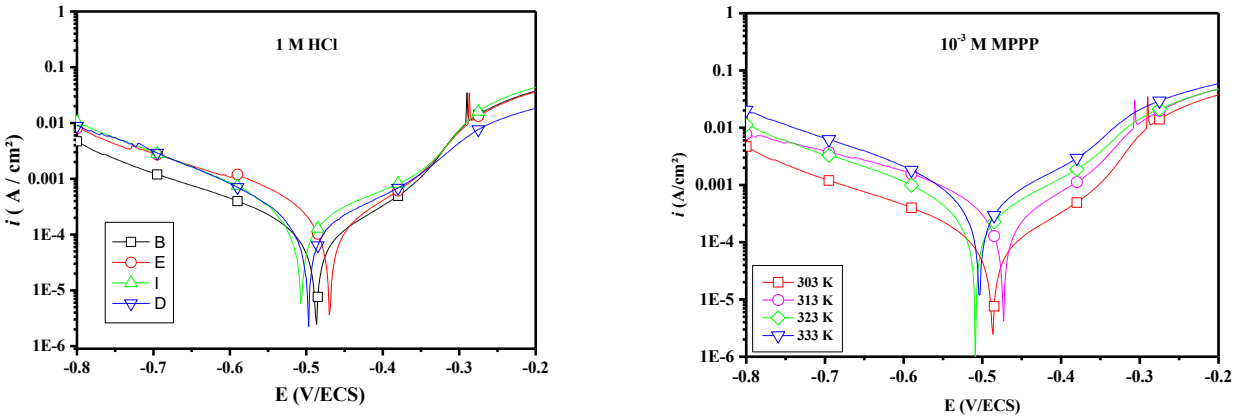

Figure 5: Potentiodynamic polarization curves of carbon steel in 1.0 M HCl (a) and in the presence of 1×10^{-3} M MPPP (b) at different temperatures.

Table 3: The influence of temperature on the electrochemical parameters for carbon steel electrode immersed in 1.0 M HCl and 1.0 M HCl + 1×10^{-3} M MPPP.

Inhibitor	Temperature (K)	E_{corr} (mV/SCE)	βa (mV dec^{-1})	-βc (mV dec^{-1})	i_{corr} (µA cm^{-2})	η_{PDP} (%)
Blank	303	-450	95.9	124.9	513	-
	313	-445	70.3	64.4	859	-
	323	-455	77.4	79.2	988	-
	333	-456	72.6	76.3	1423	-
MPPP	303	-486	78.4	119.3	35	93
	313	-473	96.5	141.3	183	78
	323	-508	127.6	150.6	251	74
	333	-503	125.6	147	413	70

The activation energy (E_a), enthalpy (ΔH^*), and entropy (ΔS^*) values shown in Table 4 were evaluated by performing PDP measurements in the temperature range of 308–338 K in the absence and presence of the optimum concentration of MPPP. The activation energy (E_a), enthalpy (ΔH^*), and entropy (ΔS^*) were calculated using the following equations:

$$i_{corr} = A\ exp\left(\frac{-E_a^*}{RT}\right) \quad (14)$$

$$i_{corr} = \frac{RT}{Nh}\ exp\left(\frac{\Delta H_a^*}{R}\right) exp\left(-\frac{\Delta S_a^*}{RT}\right) \quad (15)$$

where E_a is the activation energy for corrosion of carbon steel in 1 M HCl, R is the gas constant, A is the Arrhenius pre-exponential factor, T is the absolute temperature, h is Plank's constant and N is Avogadro's number.

A plot of the corrosion current density ln i_{corr} vs. 1000/T resulted in straight lines, as shown in Fig. 6. The values of E_a in 1 M HCl in the absence and presence of the inhibitor were determined from the slope. A plot of ln (i_{corr} /T) against 1000/T, as shown in Fig. 6, shows straight lines with a slope of ($-\Delta H^*/R$) and an intercept of [(ln (R/Nh)) + ($\Delta S^*/R$)], from which the values of ΔH^* and ΔS^* were calculated.

The apparent increase in E_a and ΔH^* suggested the creation of an energy barrier to the corrosion reaction in the presence of the inhibitor. The higher value of ΔS^* for the inhibited solution might be the result of the adsorption of the MPPP molecules in the 1 M HCl solution (quasi substitution)[48].

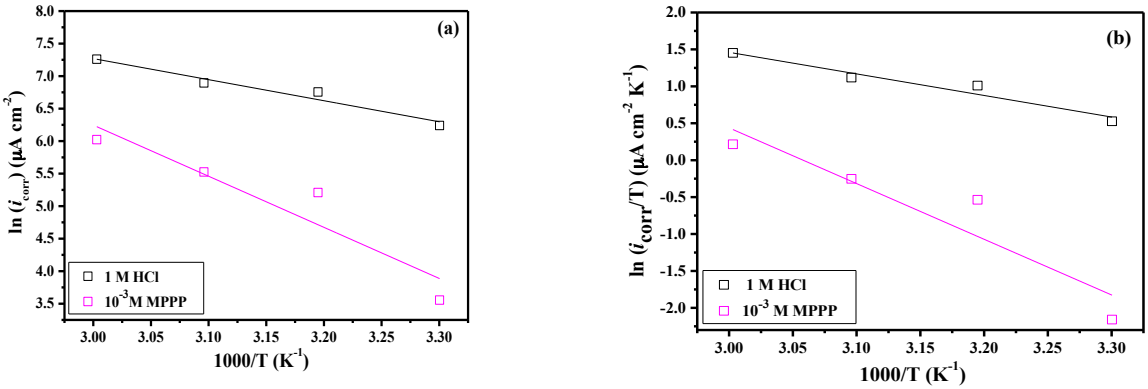

Figure 6: Arrhenius plots (a) and Transition state plots (b) for mild steel in 1M HCl and 1M HCl+1×10^{-3} M MPPP

Table 4: Corrosion kinetic parameters for mild steel in 1M HCl in the absence and presence of 1×10^{-3} M MPPP.

Inhibitor	E_a^* (kJ/mol)	ΔH_a^* (kJ/mol)	ΔS_a^* (J mol-1 K^{-1})	$E_a^* - \Delta H_a^*$
1 M HCl	26.91	24.26	-112.48	2.6
1×10^{-3} MMPPP	65.33	62.69	-1.24	2.6

3.3 Adsorption isotherm and thermodynamic adsorption parameters

The surface coverage (θ) values corresponding to various concentrations of inhibitor have been used to explain the correct isotherm for adsorption process. Surface coverage (θ) values were attempted to fit to different isotherms such as Freundlich, Temkin, Langmuir and Frumkin isotherms. The best fit was obtained with Langmuir isotherm which is represented by the following equation[49]:

$$\frac{C}{\theta} = \frac{1}{K_{ads}} + C \qquad (16)$$

where K_{ads} is the adsorption equilibrium constant, and C_{inh} is the inhibitor concentration. Straight lines were obtained when we plot C_{inh}/θ against C_{inh} (Fig. 7) which suggested the adsorption of inhibitor on the carbon steel surface followed Langmuir adsorption isotherm.

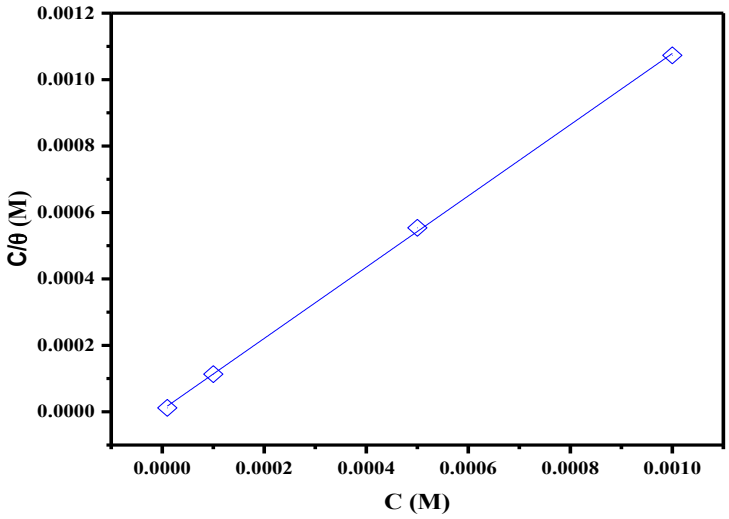

Figure 7: Langmuir adsorption of MPPP on the mild steel surface in 1.0 M HCl solution at 303K.

The adsorption equilibrium constant (K_{ads}) and free energy of adsorption (ΔG_{ads}) were calculated using the Equation[50]:

$$\Delta G_{ads} = -RT\ln(K_{ads} * C_{solvent}) \qquad (17)$$

Where: $C_{solvent}$is the molar concentration of solvent (For H_2O is 55.5mol L^{-1}). R is universal gas constant,T is the absolute temperature.

The values of K_{ads} and ΔG_{ads} were calculated and are listed in Table 5. It is mentioned in various literature that the values of ΔG_{ads} up to −20 kJ mol^{-1} are consistent with electrostatic interaction between charged inhibitor molecules and a charged metal (physical adsorption), while those nearly −40 kJ mol^{-1} or higher corresponds to the charge sharing or charge transfer from the inhibitor molecules to the metal surface to form a co-ordinate type bond (chemical adsorption)[51]. The calculated value of ΔG_{ads} for studied inhibitor is -44.44 kJ mol^{-1}. This suggests that the chemical mode of adsorption may be the predominance mode of action. Higher values of K_{ads} mean better inhibition efficiency of an inhibitor and strong interaction between the inhibitor molecules and the metal surface[52,53].

Table 5: The adsorption parameters for the corrosion of carbon steel in 1.0 M HCl at 303K

Inhibitor	Slope	$K_{ads}(M^{-1})$	R^2	ΔG_{ads}(kJ/mol)
MPPP	1.06	152858	0.999	- 44.44

3.4.Quantum chemical calculation

3.4.1. Global reactivity descriptors

The quantum chemical calculation plays a vital role in selecting the best corrosion inhibitor with required structural characteristics. This theoretical approach helps to find the corrosion inhibition effectiveness which depends on the molecular structure. The calculated quantum chemical parameters related to the inhibition effect of MPPP such as the energy of the highest occupied molecular orbital (E_{HOMO}), the energy of the lowest unoccupied molecular orbital (E_{LUMO}), the gap energy ΔE_{gap}, and the fraction of electron transferred ΔN were calculated and listed in Table 6. The optimized geometry, HOMO and LUMO of MPPP were shown in Fig. 8.

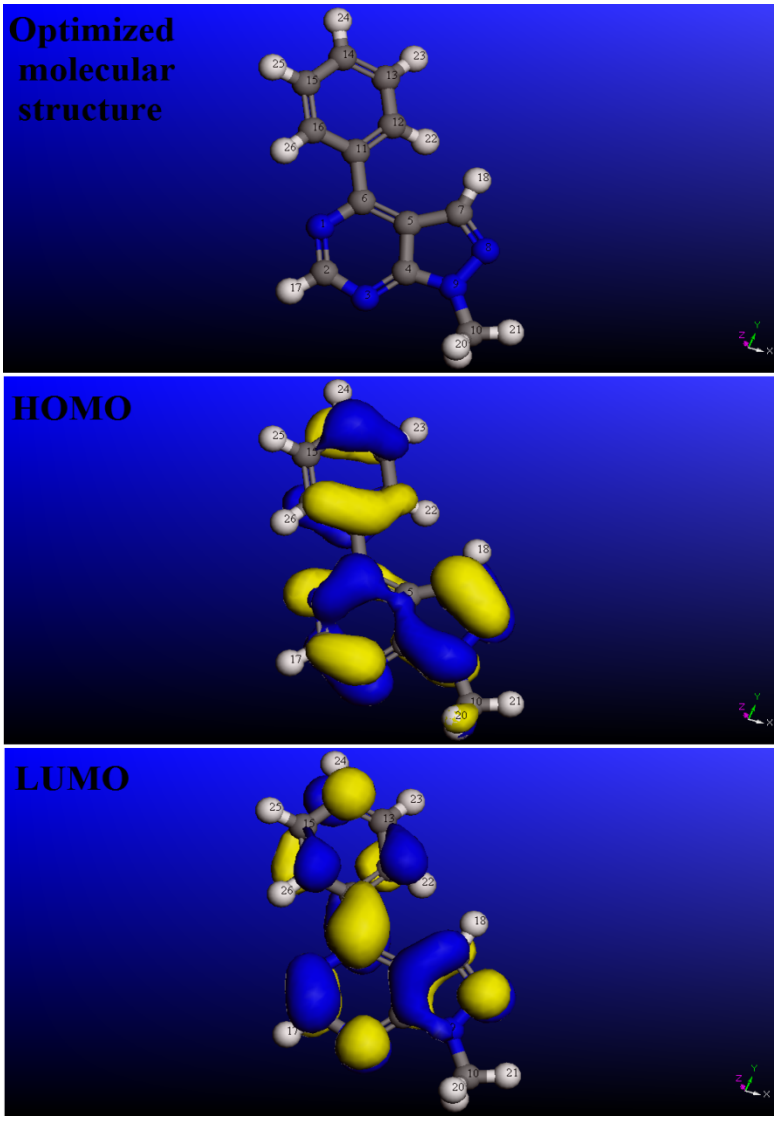

Figure 8: Optimized molecular structure and frontier orbitals distribution HOMO and LUMO of MPPP.

In MPPP, it is seen from the HOMO and LUMO that the electron density is distributed over the entire molecule. It can be concluded from these observations that the nitrogen atoms and π system are mainly responsible for the interaction with metal surface.The quantum chemical parameters such as the energy of the HOMO (E_{HOMO}), energy of the LUMO (E_{LUMO}) can be utilized to understand the adsorption phenomenon of the inhibitor on the metal surface. Table 6 reports the quantum chemical parameters investigated in this work.

Table 6: Calculated quantum chemical parameters of the inhibitor molecule.

Quantum Parameters	E_{HOMO} (eV)	E_{LUMO} (eV)	ΔE_{L-H} (eV)	ΔN
MPPP	-4.98	-1.83	3.14	0.44

The high value of E_{HOMO} (-4.98 eV) is likely to indicate a tendency of the molecule MPPP to donate electron to appropriate acceptor molecules with low energy or empty electron orbital. The lower the value (-1.83 eV) of E_{LUMO}, the more probable it is that the molecule would accept electrons [54]. The transfer of electron from inhibitor molecule to the metallic surface will occur when $\Delta N > 0$ [55]. Elnga*et al.* have reported that there is an increase in electron donation capability of inhibitor molecules when the ΔN value is less than 3.6[56]. From Table 6, it is observed that all the calculated ΔN= 0.44values are positive and lower than 3.6, which strongly indicates that the inhibitor molecules have the capability in donating electrons to the vacant d-orbital of metal.

3.4.2. Actives sites: the $f^{\pm}$Fukui function

Fukui functions are used to measure the local reactivity of the inhibitors molecules and indicate their chemical reactivity for nucleophilic and electrophilic nature[57,58]. Using a scheme of finite difference approximations, this procedure condenses the values around each atomic site into a single value that characterizes the atom in the molecule.

The preferred site for nucleophilic attack is the atom in the molecule where the value of f^+ is the highest while the preferred site for electrophilic attack is the atom in the molecule where the value of f^- is the highest[59]. The values of calculated Fukui functions based on Mulliken population analysis are given in Table 7. In this inhibitor, atoms N3, C6, and N8 respectively, present the highest values of f_k^+, where are the most susceptible sites for nucleophilic attacks. On the other hand, N3, C7, and N8 are the susceptible sites for electrophilic attacks as they present the highest values of f_k^-.

Table 7: The values of the Fukui functions for MPPP.

Atom	f^+	f^-
N (1)	0.043	0.059
C (2)	0.043	0.038
N (3)	**0.098**	**0.080**
C (4)	0.026	0.026
C (5)	0.013	0.002
C (6)	**0.089**	0.031
C (7)	0.038	**0.063**
N (8)	**0.091**	**0.080**
N (9)	0.010	0.043
C (10)	-0.019	-0.024
C (11)	-0.004	0.017
C (12)	0.028	0.014
C (13)	0.010	0.019
C (14)	0.046	0.041
C (15)	0.013	0.012
C (16)	0.025	0.026

3.5. MD simulations

Recently, MD simulation has emerged as a modern tool to investigate the adsorption behavior of the inhibitor molecule on the metallic surface. MD simulation can reasonably predict the most favorable configuration of the adsorbed inhibitor molecule on the Fe-surface. Thus for a better insightfulness in the adsorption phenomenon,

our inhibitor (MPPP) has been considered to act on the Fe (110) surface to determine the suitable and adorable adsorption configuration. In this context, when the temperature and energy of the system reaches in equilibrium, $E_{interaction}$ and $E_{binding}$ between the inhibitor and Fe (110) surface can be calculated. The calculated $E_{interaction}$ and $E_{binding}$ values are -745.08 kJ/mol and 745.08 kJ/mol respectively. The best adsorption configuration of the inhibitor over Fe(110) surface as well as the close contact between those are depicted in Fig. 9. It is clearly observed that the inhibitor molecule is adsorbed on the Fe (110) surface with almost parallel or flat disposition. This flat orientation is possibly due to the formation of coordination and back-bonding between the inhibitor and metal surface. It is also evident herein that the presence of unoccupied metal d-orbitals will prefer to accept electron from the adsorbed inhibitor molecule. The strong adsorption between the inhibitor and the Fe (110) surface is confirmed from the large interaction energy value[51]. MD simulation results are in excellent agreement with the results coming out from quantum chemical calculations as well as from experimental findings.

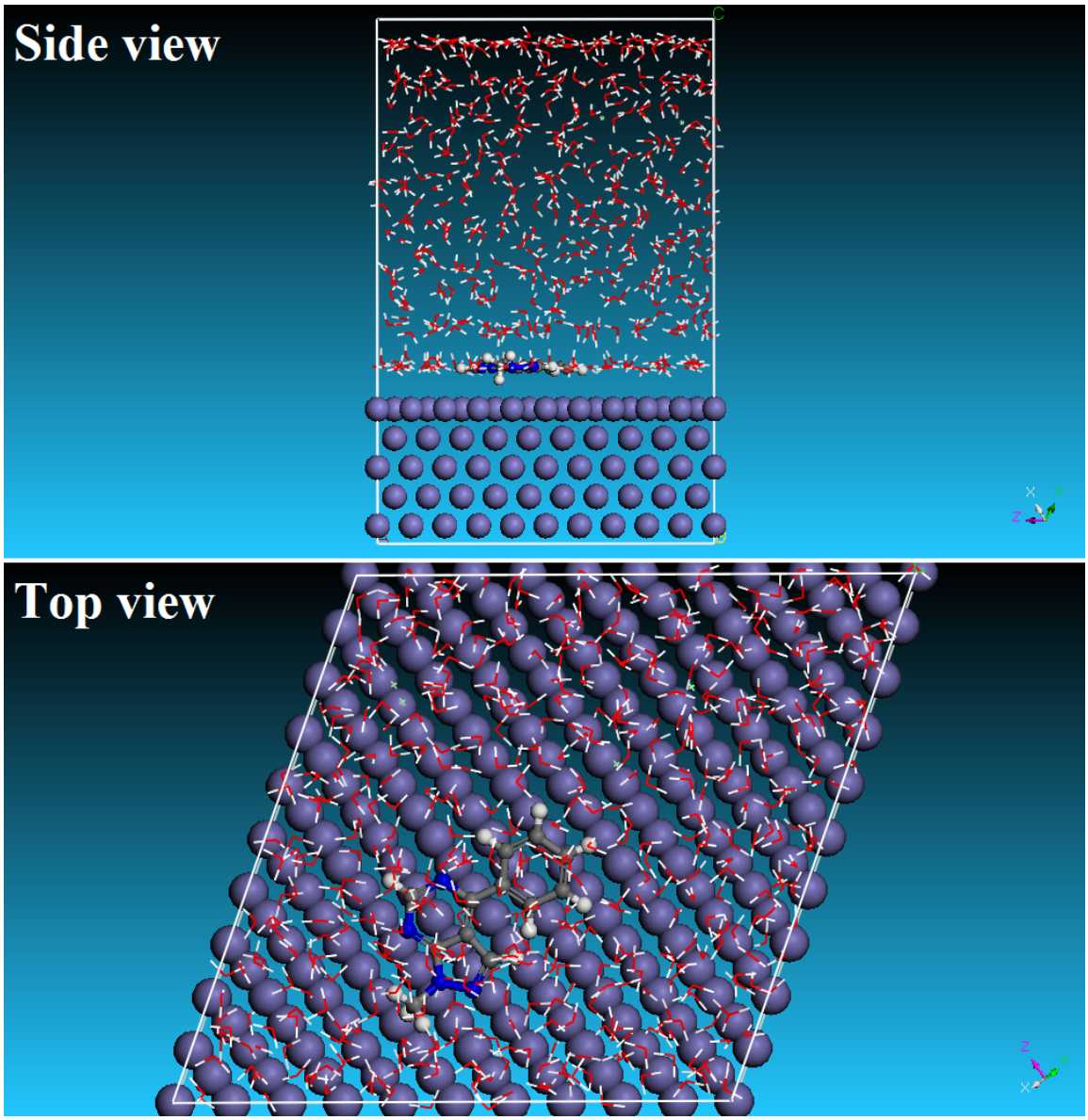

Figure9: Equilibrium adsorption configuration of studied inhibitor on the Fe (110) plane obtained by MD simulation.

Conclusion

In this present investigation, the interaction between the 1-methyl-4-phenyl-1*H*-pyrazolo[3,4-d]pyrimidine (MPPP) and mild steel surface has been successfully investigated by a combined experimental and theoretical investigation. According to experimental findings, the MPPP compound is a good corrosion inhibitor for mild

steel in 1.0 M HCl solution and its performance depends on its concentration and its molecular structure. PDP measurements indicate that the MPPP acts as a mixed type inhibitor. EIS measurements also indicate that the inhibitor addition increases the polarization resistance and show that the inhibitive performance depends on molecules adsorption on metallic surface. Quantum chemical and MD simulations approaches were adequately used to explain the correlation between the mild steel corrosion inhibition and molecular structure of compound.

References:

1. R. Salghi, S. Jodeh, E.E. Ebenso, H. Lgaz, D. Ben Hmamou, I.H. Ali, M. Messali, B. Hammouti, N. Benchat, *Int. J. Electrochem. Sci.* 12 (2017) 3309.
2. T. Laabaissi, H. Lgaz, H. Oudda, F. Benhiba, H. Zarrok, A. Zarrouk, A. El Midaoui, B. Lakhrissi, R. Touir, *J. Mater. Environ. Sci.* 8 (2017) 1054
3. M. Messali, H. Lgaz, R. Dassanayake, R. Salghi, S. Jodeh, N. Abidi, O. Hamed, *J. Mol. Struct.* 1145 (2017) 43.
4. R. Salghi, S. Jodeh, E.E. Ebenso, H. Lgaz, D. Ben Hmamou, M. Belkhaouda, I.H. Ali, M. Messali, B. Hammouti, S. Fattouch, *Int. J. Electrochem. Sci.* 12 (2017) 3283
5. H. Lgaz, K. Subrahmanya Bhat, R. Salghi, Shubhalaxmi, S. Jodeh, M. Algarra, B. Hammouti, I.H. Ali, A. Essamri, *J. Mol. Liq.* 238 (2017) 71.
6. L. Afia, O. Hamed, M. Larouj, H. Lgaz, S. Jodeh, R. Salghi, (2017). doi:10.1007/s12666-017-1094-x.
7. Y. El Aoufir, Y. El Bakri, H. Lgaz, A. Zarrouk, R. Salghi, I. Warad, Y. Ramli, A. Guenbour, E.M. Essassi, H. Oudda, *J. Mater. Environ. Sci*. 8 (2017) 3290.
8. V. Rajeswari, D. Kesavan, M. Gopiraman, P. Viswanathamurthi, K. Poonkuzhali, T. Palvannan, *Appl. Surf. Sci.* 314 (2014) 537.
9. M. Shabani-Nooshabadi, F.S. Hoseiny, Y. Jafari, *Metall. Mater. Trans. A*. 46 (2015) 293.
10. M. Belayachi, H. Serrar, A. El Assyry, H. Oudda, S. Boukhris, M. Ebn Touhami, A. Zarrouk, B. Hammouti, Eno E. Ebenso, A. El Midaoui, Int. J. Electrochem. Sci. 10 (2015) 3038.
11. A. Ghazoui, R. Saddik, N. Benchat, B. Hammouti, M. Guenbour, A. Zarrouk, M. Ramdani, Der Pharm. Chem. 4 (2012) 352.
12. H. Zarrok, R. Saddik, H. Oudda, B. Hammouti, A. El Midaoui, A. Zarrouk, N. Benchat, M. Ebn Touhami, Der Pharm. Chem. 3 (2011) 272.
13. A. Zarrouk, B. Hammouti, R. Touzani, S.S. Al-Deyab, M. Zertoubi, A. Dafali, S. Elkadiri, Int. J. Electrochem. Sci. 6 (2011) 4939.
14. A. Zarrouk, B. Hammouti, A. Dafali, H. Zarrok, Der Pharm. Chem. 3 (2011) 266.
15. A. Ghazoui, A. Zarrouk, N. Bencaht, R. Salghi, M. Assouag, M. El Hezzat, A. Guenbour, B. Hammouti, J. Chem. Pharm. Res. 6 (2014) 704.
16. H. Zarrok, A. Zarrouk, R. Salghi, H. Oudda, B. Hammouti, M. Assouag, M. Taleb, M. Ebn Touhami, M. Bouachrine, S. Boukhris, J. Chem. Pharm. Res. 4 (2012) 5056.
17. H. Zarrok, A. Zarrouk, R. Salghi, M. Assouag, B. Hammouti, H. Oudda, S. Boukhris, S.S. Al Deyab, I. Warad, Der Pharm. Lett. 5 (2013) 43
18. M. Belayachi, H. Serrar, H. Zarrok, A. El Assyry, A. Zarrouk, H. Oudda, S. Boukhris, B. Hammouti, E.E. Ebenso, A. Geunbour, Int. J. Electrochem. Sci. 10 (2015) 3010.
19. A. Zarrouk, H. Zarrok, R. Salghi, R. Touir, B. Hammouti, N. Benchat, L.L. Afrine, H. Hannache, M. El Hezzat, M. Bouachrine, J. Chem. Pharm. Res. 5 (2013) 1482.
20. H. Zarrok, A. Zarrouk, R. Salghi, M. Ebn Touhami, H. Oudda, B. Hammouti, R. Touir, F. Bentiss, S.S. Al-Deyab, Int. J. Electrochem. Sci. 8 (2013) 6014.
21. D. Ben Hmamou, M.R. Aouad, R. Salghi, A. Zarrouk, M. Assouag, O. Benali, M. Messali, H. Zarrok, B. Hammouti, J. Chem. Pharm. Res. 4 (2012) 34984.
22. A.J. Bard, M. Stratmann, P.R. Unwin, 4, Wiley-VCh, 2003.
23. R. Solmaz, *Corros. Sci.* 79 (2014) 169
24. H. Lgaz, R. Salghi, K. Subrahmanya Bhat, A. Chaouiki, Shubhalaxmi, S. Jodeh, *J. Mol. Liq*. 244 (2017) 154.

25. R. Kumar, S. Chahal, S. Kumar, S. Lata, H. Lgaz, R. Salghi, S. Jodeh, *J. Mol. Liq.* 243 (2017) 439.
26. Materials Studio, Revision 6.0, Accelrys Inc., San Diego, USA, 2013.
27. B. Delley, *J. Chem. Phys.* 92 (1990) 508.
28. B. Delley, *J. Chem. Phys.* 113 (2000) 7756.
29. M.J. Dewar, W. Thiel, *J. Am. Chem. Soc*. 99 (1977) 4899.
30. R.G. Pearson, *Inorg. Chem*. 27 (1988) 734.
31. V. Sastri, J. Perumareddi, *Corrosion.* 53 (1997) 617.
32. I. Lukovits, E. Kalman, F. Zucchi, *Corrosion*. 57 (2001) 3.
33. M. Lebrini, F. Bentiss, N.-E. Chihib, C. Jama, J.P. Hornez, M. Lagrenée, *Corros. Sci.* 50 (2008) 2914.
34. Z. Cao, Y. Tang, H. Cang, J. Xu, G. Lu, W. Jing, *Corros. Sci.* 83 (2014) 292.
35. A. Kokalj, *Chem. Phys.* 393 (2012) 1.
36. R.G. Parr, W. Yang, *J. Am. Chem. Soc.* 106 (1984) 4049.
37. R.R. Contreras, P. Fuentealba, M. Galván, P. Pérez, *Chem. Phys. Lett.* 304 (1999) 405.
38. H.-L. Wang, H.-B. Fan, J.-S. Zheng, *Mater. Chem. Phys.* 77 (2003) 655.
39. M. El Azhar, B. Mernari, M. Traisnel, F. Bentiss, M. Lagrenee, *Corros. Sci.* 43 (2001) 2229.
40. K. Krishnaveni, J. Ravichandran, *J. Electroanal. Chem.* 735 (2014) 24.
41. M. Yadav, D. Behera, S. Kumar, *Surf. Interface Anal.* 46 (2014) 640.
42. S.K. Saha, A. Dutta, P. Ghosh, D. Sukul, P. Banerjee, *Phys. Chem. Chem. Phys.* 17 (2015) 5679.
43. W. Chen, S. Hong, B. Xiang, H. Luo, M. Li, N. Li, *Corros. Eng. Sci. Technol.* 48 (2013) 98.
44. N. Manimaran, S. Rajendran, M. Manivannan, S. John Mary, *Res. J. Chem. Sci.* 2 (2012) 52.
45. S. Rengamani, S. Muralidharan, M. Anbu Kulandainathan, S. Venkatakrishna Iyer, *J. Appl. Electrochem.* 24 (1994) 355.
46. I.A. Aiad, N.A. Negm, *J. Surfactants Deterg.* 12 (2009) 313.
47. A. Popova, E. Sokolova, S. Raicheva, M. Christov, *Corros. Sci.* 45 (2003) 33.
48. D.K. Yadav, B. Maiti, M. Quraishi, *Corros. Sci.* 52 (2010) 3586.
49. H. Lgaz, R. Salghi, S. Jodeh, Y. Ramli, M. Larouj, K. Toumiat, M. Quraishi, H. Oudda, W. Jodeh, *J Steel Struct Constr.* 2 (2016) 2472.
50. H. Lgaz, O. Benali, R. Salghi, S. Jodeh, M. Larouj, O. Hamed, M. Messali, S. Samhan, M. Zougagh, H. Oudda, *Pharma Chem.* 8 (2016) 172.
51. H. Lgaz, R. Salghi, S. Jodeh, B. Hammouti, *J. Mol. Liq*. 225 (2017) 271.
52. C. Verma, M.A. Quraishi, A. Singh, *J. Mol. Liq.* 212 (2015) 804.
53. C. Verma, E.E. Ebenso, I. Bahadur, I.B. Obot, M.A. Quraishi, *J. Mol. Liq.* 212 (2015) 209.
54. G. Gece, *Corros. Sci.* 50 (2008) 2981.
55. S.K. Saha, P. Banerjee, *RSC Adv.* 5 (2015) 71120.
56. M.K. Awad, M.R. Mustafa, M.M.A. Elnga, *J. Mol. Struct. Theochem.* 959 (2010) 66.
57. J. Saranya, P. Sounthari, K. Parameswari, S. Chitra, *Measurement.* 77 (2016) 175.
58. S.K. Saha, P. Ghosh, A. Hens, N.C. Murmu, P. Banerjee, *Phys. E Low-Dimens. Syst. Nanostructures.* 66 (2015) 332.
59. N. Karakus, K. Sayin, *J. Taiwan Inst. Chem. Eng.* 48 (2015) 95.

(2018) ; http://www.jmaterenvironsci.com